Electronic Supplementary Material (ESI) for Physical Chemistry Chemical Physics.

Electronic Supporting Information

Attenuated Total Reflectance Far-Ultraviolet and Deep-Ultraviolet Spectroscopy Analysis of the Electronic Structure of a Dicyanamide-Based Ionic Liquid with Li^+

Masaya Imai[a], Ichiro Tanabe[a*], Akifumi Ikehata[b], Yukihiro Ozaki[c,d] and Ken-ichi Fukui[a,e*]

[a] Department of Materials Engineering Science, Graduate School of Engineering Science, Osaka University, Toyonaka, Osaka 560-8531, Japan.
[b] National Food Research Institute, National Agriculture and Food Research Organization (NARO), Tsukuba, Ibaraki, 305-8642, Japan.
[c] Department of Chemistry, School of Science and Technology, Kwansei Gakuin University, Sanda, Hyogo, 669-1337, Japan.
[d] Toyota Physical Chemical Research Institute, Nagakute, Aichi 480-1192, Japan.
[e] Department of Photomolecular Science, Institute of Molecular Science, Myodaiji, Okazaki, Aichi 444-8585, Japan.

***Corresponding authors: E-mail addresses:**

itanabe@chem.es.osaka-u.ac.jp (I.T.) and

kfukui@chem.es.osaka-u.ac.jp (K.F.)

Contents

1. Detailed time-dependent density functional theory (TD-DFT) calculations

Table S1 Calculated transition wavelengths, oscillation strength, main initial states, and main final states of $[DCA]^-$.

Wavelength / nm	Oscillation strength	Initial state	Final state
226.76	0.0081	HOMO	LUMO
189.75	0.1784	HOMO	LUMO+6

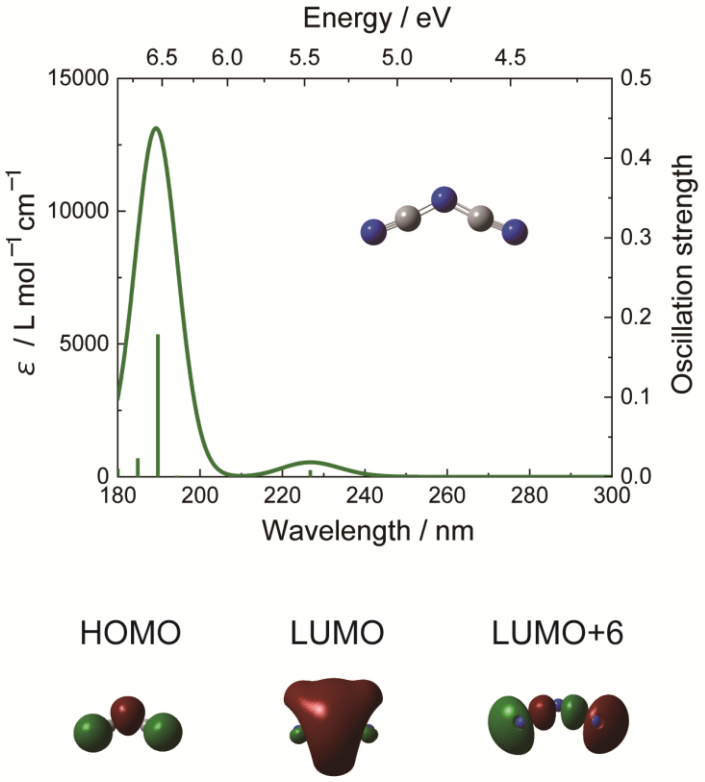

Figure S1 Calculated oscillation strengths and molar extinction coefficient (ε) of $[DCA]^-$. The molecular orbitals of the main initial and final states are presented at the bottom. This time-dependent density functional theory calculation was performed using the CAM-B3LYP/aug-cc-pVTZ basis set. The surrounding [BMP][DCA] was reflected as a continuum solvation model using the solvation model based on density-generic ionic liquid.

Table S2 Calculated transition wavelengths, oscillation strength, main initial states, and main final states of $[BMP]^+$.

Wavelength / nm	Oscillation strength	Initial state	Final state
138.44	0.0168	HOMO-1	LUMO+1
133.95	0.0429	HOMO	LUMO+1
132.86	0.0393	HOMO	LUMO+2
130.79	0.0473	HOMO-1	LUMO+1

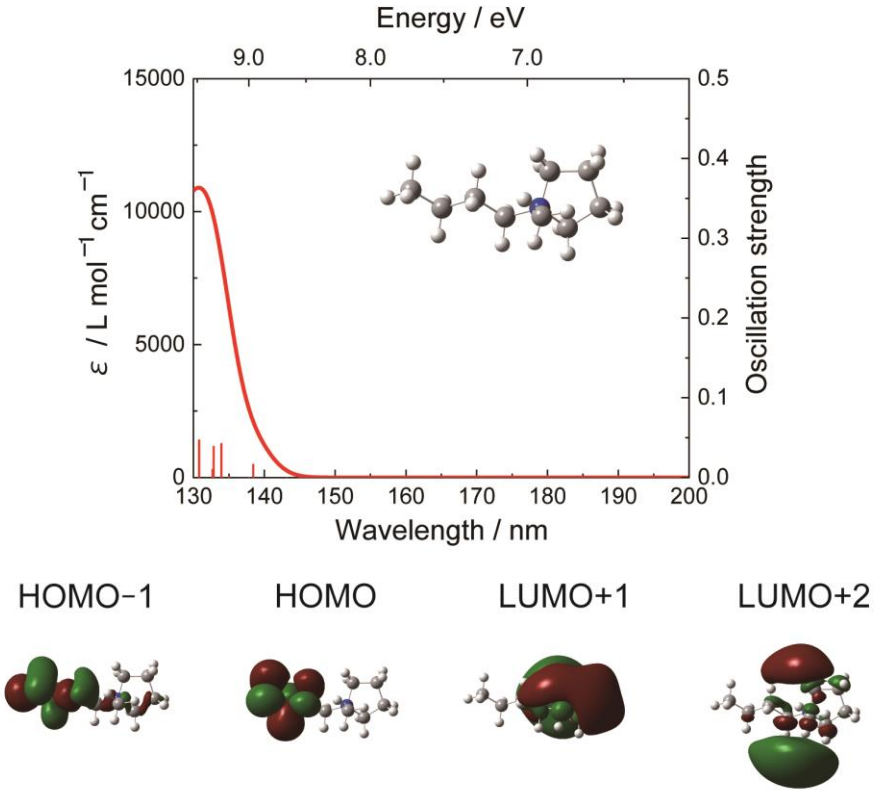

Figure S2 Calculated oscillation strengths and molar extinction coefficients (ε) of $[BMP]^+$. The molecular orbitals of the main initial and final states are illustrated at the bottom. The optimisation was performed via density functional theory using the B3LYP/aug-cc-pVTZ basis set and the vertical transitions were calculated using the time-dependent density functional theory using the CAM-B3LYP/aug-cc-pVTZ basis set. The surrounding [BMP][DCA] was reflected as a continuum solvation model using the solvation model based on density-generic ionic liquid. Our calculations indicated that the absorption bands that derived from the intramolecular electronic transitions of $[BMP]^+$ emerged below 130 nm. It was concluded that the electronic absorption of $[BMP]^+$ did not contribute to the obtained absorption spectra in the 180–300 nm spectral region.

2. Spectral decomposition using multivariable curve resolution-alternating least squares (MCR-ALS) calculations

The spectral decompositions illustrated in Figure 4 were performed using the multivariable curve resolution-alternating least squares (MCR-ALS) algorithm in the 180–250 nm spectral region. The detailed processes are presented below.

The absorption spectra of the Li-IL are illustrated in an 8 (number of concentrations of Li^+ except for 0 M) × 701 (number of absorption data) matrix ($\boldsymbol{A}$). Our goal was to decompose $\boldsymbol{A}$ into $\boldsymbol{A}_{\mathbf{IL}}$ and $\boldsymbol{A}_{\mathbf{Li[DCA]}}$, the matrices of the absorption spectra derived from $[DCA]^-$ without and with the effect of Li^+ on the levels of the electronic states, respectively:

$$\boldsymbol{A} = \boldsymbol{A}_{\mathbf{IL}} + \boldsymbol{A}_{\mathbf{Li[DCA]}}. \tag{S1}$$

We assumed that $\boldsymbol{A}_{\mathbf{IL}}$ can be expressed using the contribution vector of pure [BMP][DCA] ($\boldsymbol{t}^{\boldsymbol{x}}$) and the spectrum of pure [BMP][DCA] ($\boldsymbol{A}_{\mathbf{0}}$, black line in Figure 1(a)) utilising Eq. (S2):

$$\boldsymbol{A}_{\mathbf{IL}}^{\boldsymbol{x}} = \boldsymbol{t}^{\boldsymbol{x}}\boldsymbol{A}_{\mathbf{0}}, \tag{S2}$$

in which

$$\boldsymbol{t}^{\boldsymbol{x}} = \begin{pmatrix} t_1 \\ t_2 \\ \vdots \\ t_8 \end{pmatrix} = \boldsymbol{I} - \frac{x}{c_{\mathrm{IL},0}}\boldsymbol{c}_{\mathbf{Li}}, \qquad \boldsymbol{c}_{\mathbf{Li}} = \begin{pmatrix} c_{\mathrm{Li},1} \\ c_{\mathrm{Li},2} \\ \vdots \\ c_{\mathrm{Li},8} \end{pmatrix}, \qquad \boldsymbol{I} = \begin{pmatrix} 1 \\ 1 \\ \vdots \\ 1 \end{pmatrix}, \tag{S3}$$

where $c_{\mathrm{IL},0}$ is the molar concentration of $[DCA]^-$ in pure [BMP][DCA] (4.9 M), the numbers from 1 to 8 are the experiment numbers using [BMP][DCA] and different Li^+ concentrations in the range of 0.054–0.27 M, and x is the test electronic coordination number (ECN) of $[DCA]^-$ with electronic states affected by Li^+. For each test ECN ($3 \le x \le 9$), $\boldsymbol{A}_{\mathbf{IL}}^{\boldsymbol{x}}$ was calculated using Eqs. (S2) and (S3). Furthermore, $\boldsymbol{\Delta A}^{\boldsymbol{x}}$ can be calculated as follows:

$$\boldsymbol{\Delta A}^{\boldsymbol{x}} = \boldsymbol{A} - \boldsymbol{t}^{\boldsymbol{x}}\boldsymbol{A}_{\mathbf{0}}. \tag{S4}$$

Using the MCR-ALS algorithm for several x values ($3 \le x \le 9$), $\boldsymbol{\Delta A}^{\boldsymbol{x}}$ was decomposed into spectral profiles ($\boldsymbol{S}^{\boldsymbol{x}}$) and contribution profiles ($\boldsymbol{C}^{\boldsymbol{x}}$) as follows:

$$\boldsymbol{\Delta A}^{\boldsymbol{x}} = \boldsymbol{C}^{\boldsymbol{x}}\boldsymbol{S}^{\boldsymbol{xT}} + \boldsymbol{E}, \tag{S5}$$

$\boldsymbol{S}^{\boldsymbol{xT}}$ is the transposed matrix of $\boldsymbol{S}^{\boldsymbol{x}}$. The decomposed matrices were determined via the singular value decomposition and the ALS method, by minimising the residual error matrix ($\boldsymbol{E}$) in a least square sense under the condition that all signs in $\boldsymbol{S}^{\boldsymbol{x}}$ were positive. All MCR-ALS calculations were conducted using the

Unscrambler® X 10.5.1 software. $\boldsymbol{\Delta A^x}$ was decomposed into two components: α and β, using MCR-ALS calculations. The obtained $\boldsymbol{S^x}$ ($\boldsymbol{S_\alpha^x}$ and $\boldsymbol{S_\beta^x}$) and $\boldsymbol{C^x}$ ($\boldsymbol{C_\alpha^x}$ and $\boldsymbol{C_\beta^x}$) spectra are presented in Figures 4 and S3, respectively. Moreover, $\boldsymbol{\Delta A^x}$ can be expressed as a sum:

$$\boldsymbol{\Delta A^x} = \boldsymbol{C_\alpha^x S_\alpha^{xT}} + \boldsymbol{N^x} \left(\boldsymbol{N^x} \coloneqq \boldsymbol{C_\beta^x S_\beta^{xT}}\right). \quad (S6)$$

Using Eqs. (S4) and (S6), $\boldsymbol{A}$ was decomposed into three terms:

$$\boldsymbol{A} = \boldsymbol{A_{\mathrm{IL}}^x} + \boldsymbol{C_\alpha^x S_\alpha^{xT}} + \boldsymbol{N^x}, \quad (S7)$$

and each of the terms in Eq. (S7) is presented in Figures 5 and S4.

We observed two tendencies. First, Figures 4 and S3 illustrate that $\boldsymbol{C_\alpha^x}$ became increasingly proportional with the concentration of Li^+ as x increased, which is described using Eq. (S8):

$$\boldsymbol{C_\alpha^x} = k_x \boldsymbol{c_{\mathrm{Li}}} \ (k_x : constant), \quad (S8)$$

and the fitting results and coefficients of determination (R^2) are also presented in these figures. Second, the contribution of the other spectra matrix ($\boldsymbol{N^x}$) to $\boldsymbol{A}$ (Figures 5 and S4) decreased as x increased. The quantitative spectral contributions of $\boldsymbol{N^x}$ to $\boldsymbol{A}$ were defined as a noise ratio, as follows:

$$Noise\ ratio = \frac{\sum_{n=1}^{8} \int_{180}^{250} |\boldsymbol{N_n^x}| d\lambda}{\sum_{n=1}^{8} \int_{180}^{250} |\boldsymbol{A_n}| d\lambda}. \quad (S9)$$

When its contribution was negligible, $\boldsymbol{N^x}$ could be ignored. Therefore, we successfully separated $\boldsymbol{A}$ into $\boldsymbol{t^x A_0}$ (the absorption spectra matrix of pure [BMP][DCA]) and $\boldsymbol{c_{Li}\overline{A^x}}$ (the absorption spectra matrix of $[DCA]^-$ affected by Li^+ or including those of pure):

$$\boldsymbol{A} = \boldsymbol{t^x A_0} + \boldsymbol{c_{\mathrm{Li}}\overline{A^x}} \ (\boldsymbol{\overline{A^x}} = k_x \boldsymbol{S_\alpha^{xT}}). \quad (S10)$$

Figure S5 depicts the relationship between the noise ratios and R^2 for each x. If Eq. (S10) is satisfied at the minimum x, it corresponds to ECN because $\boldsymbol{c_{Li}\overline{A^x}}$ can be simply expressed by absorption spectra of $[DCA]^-$ affected by Li^+. The correlational plot (Figure S5) converges at x = 5, suggesting that ECN is 5.

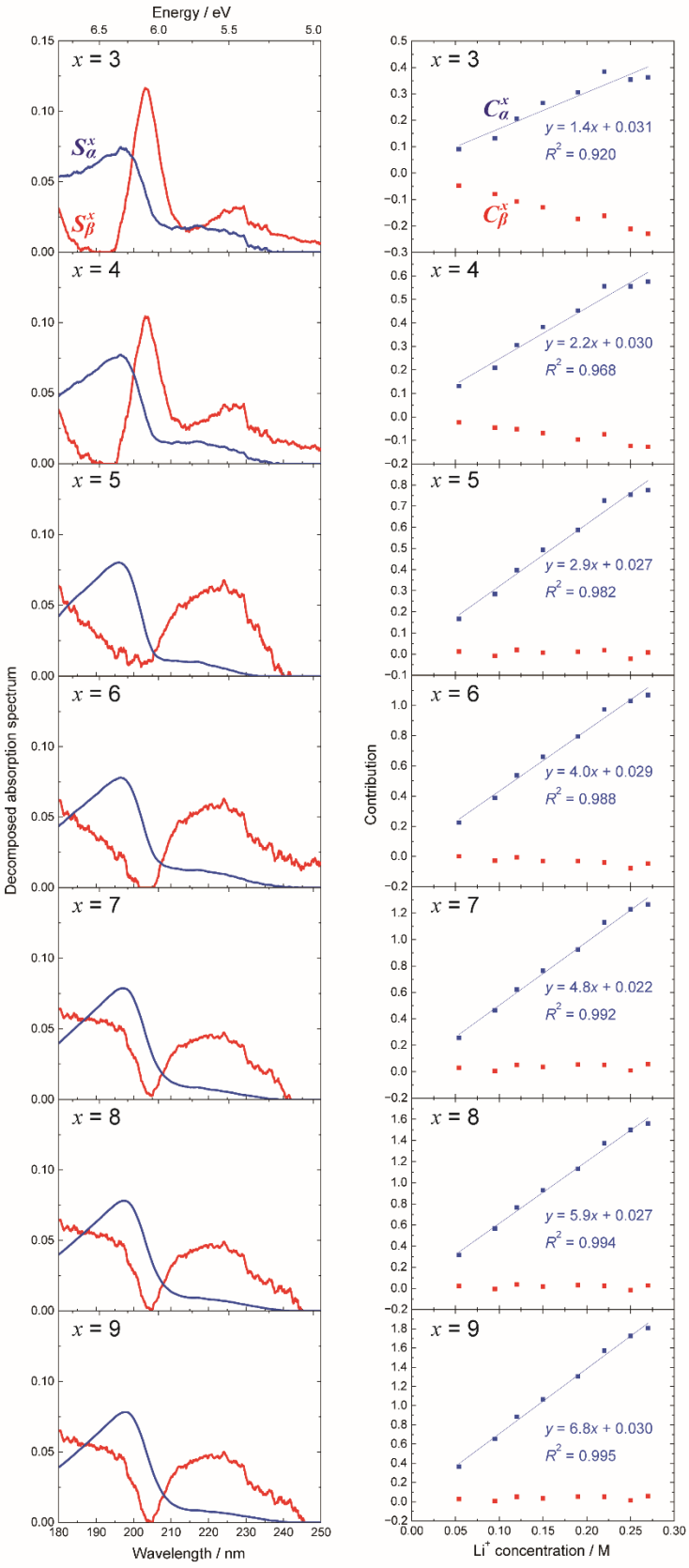

Figure S3 Decomposition of $\boldsymbol{\Delta A^x}$ into two absorption spectra ($\boldsymbol{S_\alpha^x}$ and $\boldsymbol{S_\beta^x}$) and two contributions ($\boldsymbol{C_\alpha^x}$ and $\boldsymbol{C_\beta^x}$) using the multivariable curve resolution–alternating least squares algorithm for each test ECN (x). All $\boldsymbol{S_\alpha^x}$ and $\boldsymbol{S_\beta^x}$ spectra were unit-vector normalised. The results of the linear fittings and the coefficients of determination (R^2) are also illustrated.

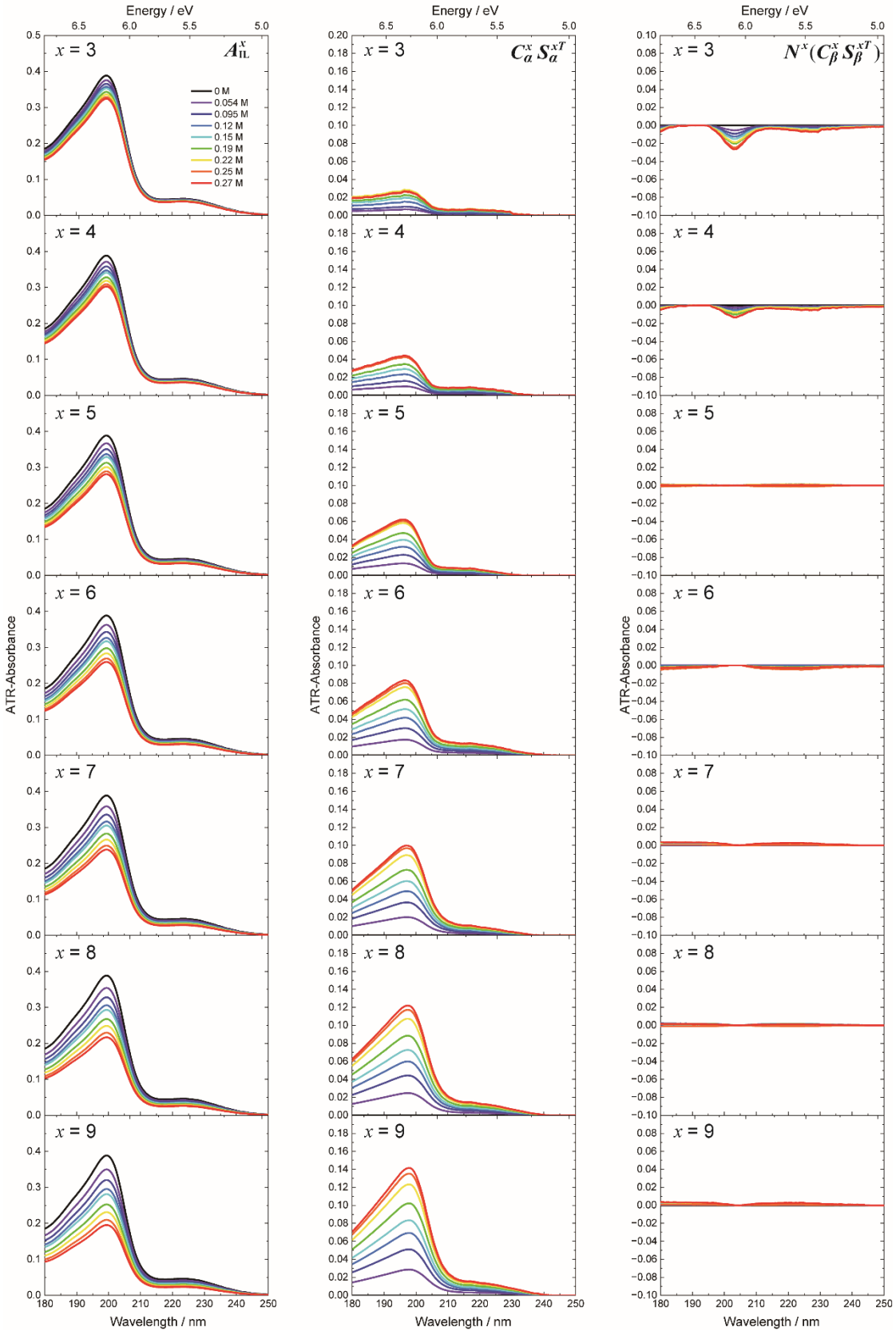

Figure S4 The terms of the absorption spectra in Eq. (S7): $\boldsymbol{A^x_{IL}(t^x A_0)}$, $\boldsymbol{C^x_\alpha S^{xT}_\alpha}$, and $\boldsymbol{N^x(C^x_\beta S^{xT}_\beta)}$ evaluated for each test ECN (x). The coloured lines represent different concentration of Li^+. The noise ratios in Eq. (S9) were determined by integrating the absorption spectra of $\boldsymbol{N^x(C^x_\beta S^{xT}_\beta)}$ with absolute values.

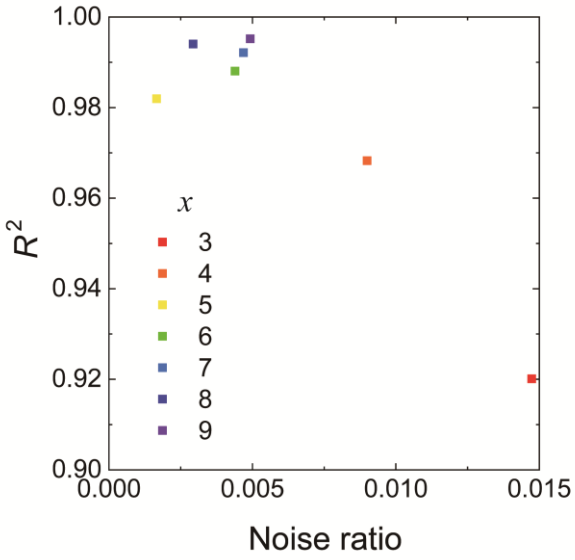

Figure S5 Relationship between noise ratios and coefficients of determination (R^2) of $\boldsymbol{C_\alpha^x}$ for various test ECN ($3 \leq x \leq 9$) illustrated as coloured dots in the legend.

3. Distance-dependent TD-DFT calculations of Li[DCA]$^{-}$

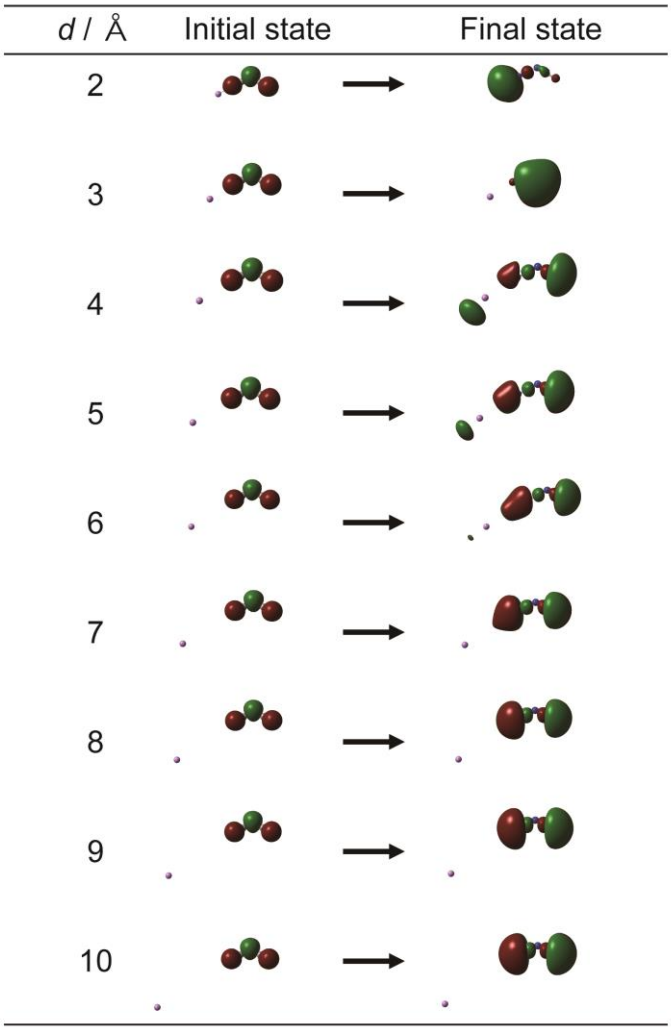

Figure S6 Results of time-dependent density functional theory calculations for the intermolecular distance (*d*) between Li^+ and the nearest terminal N atom of $[DCA]^-$. The intermolecular distances between Li^+ and the nearest terminal N atom of $[DCA]^-$ were changed from 2 to 10 Å along the N–CN bond of the $[DCA]^-$ using 1 Å steps and the other geometries of Li[DCA] illustrated in Figure 2(a) were maintained. Main initial and final molecular orbitals were extracted.

4. Residence autocorrelation function

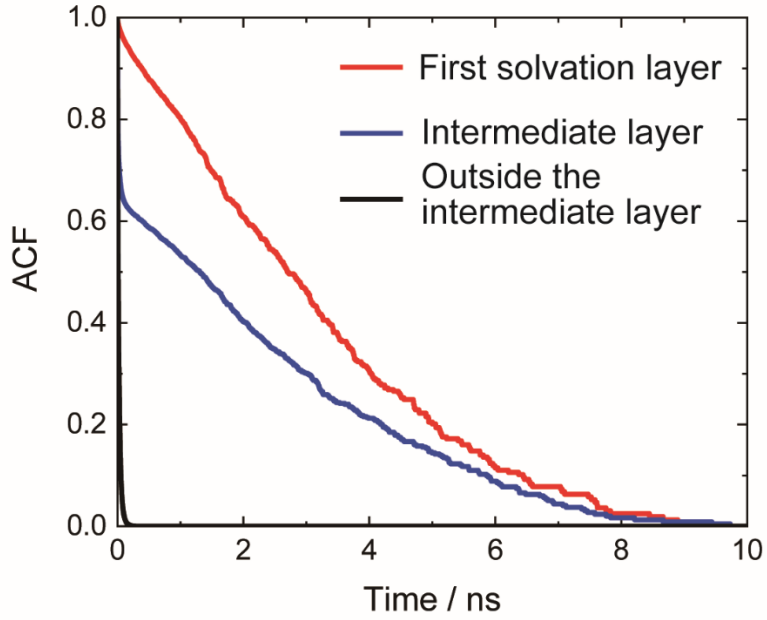

Figure S7 Averaged residence autocorrelation functions (ACF) of the terminal N atoms in the first solvation layer ($0 \leq r \leq 3.32$ Å), intermediate layer ($3.32 \leq r \leq 7.00$ Å), and outside the intermediate layer ($7.00 \leq r \leq 10.0$ Å). The depicted AFCs were calculated as the averaged values of three ACFs obtained in 0−10, 10−20, 20−30 ns.